Payri, R.; Gimeno, J.; Marti-Aldaravi, P.; Martínez-García, M. (2021). Validation of a three-phase Eulerian CFD model to account for cavitation and spray atomization phenomen. Journal of the Brazilian Society of Mechanical Sciences and Engineering. 43(4):1-15. https://doi.org/10.1007/s40430-021-02948-z

Journal of the Brazilian Society of Mechanical Sciences and Engineering manuscript No.
(will be inserted by the editor)

Validation of a three-phase Eulerian CFD model to account for cavitation and spray atomization phenomena

Raúl Payri · Jaime Gimeno · Pedro Martí-Aldaraví · María Martínez

Received: date / Accepted: date

Abstract Cavitation phase change phenomenon appears in many engineering applications, often eroding and damaging surfaces, so deteriorating the performance of devices. Therefore, it is a phenomenon of great interest for the research and industry communities. In this work, three different cavitation models, the Homogeneous Relaxation Model (HRM), the Schnerr and Sauer, and the Kunz, are implemented in a Eulerian multiphase homogeneous flow Computational Fluid Dynamics (CFD) solver previously developed for simulating fully atomized sprays. The improved solver can be used then to study not only cases with cavitation, such a hydrofoil, but also situations where cavitation occurs together with liquid atomization, such as high pressure injection systems. Validation of this solver is carried out for three different cases under diverse operating conditions: a two-dimmensional throttle, a hydrofoil and a single-hole fuel injector. The Reynolds-Averaged Navier-Stokes (RANS) approach is

The equipment and resources used in this work have been partially supported by the Universitat Politècnica de València in the framework of the PAID-06-18 program (reference SP20180170). Additionally, the Ph.D. student María Martínez has been funded by a grant from the Government of Generalitat Valenciana with reference ACIF/2018/118 and financial support from The European Union.

R. Payri
CMT-Motores Térmicos, Universitat Politècnica de València, Valencia, Spain
E-mail: rpayri@mot.upv.es
ORCID: 0000-0001-7428-5510

J. Gimeno
CMT-Motores Térmicos, Universitat Politècnica de València, Valencia, Spain
E-mail: jaigigar@mot.upv.es
ORCID: 0000-0003-3317-9994

P. Martí-Aldaraví
CMT-Motores Térmicos, Universitat Politècnica de València, Valencia, Spain
E-mail: pedmar15@mot.upv.es
ORCID: 0000-0003-4650-4004

M. Martínez
CMT-Motores Térmicos, Universitat Politècnica de València, Valencia, Spain
E-mail: mamar50m@mot.upv.es
ORCID: 0000-0002-0514-7592

R. Payri, J. Gimeno, P. Martí-Aldaraví, M. Martínez, "Validation of a three-phase Eulerian CFD model to account for cavitation and spray atomization phenomena", *Journal of the Brazilian Society of Mechanical Sciences and Engineering*, 43(228), pp. 1-15, 2021. DOI:0.1007/s40430-021-02948-z.

employed for taking into account the turbulence effects. Simulation results are compared to experimental data available in the literature. Among the tested cavitation models, the HRM is the one that provides the best accuracy in the three validation cases. Nevertheless, the onset of cavitation and the area occupied by the vapor cavities are always underpredicted, by all cavitation models in all validation cases. This can be associated to the unsteady and turbulent nature of the cavitation phenomenon. Even so, the computational prediction of several parameters, such as mass flow rate through the nozzles or spray spreading angle, has an error below 5-10%, which proves the capabilities of the solver.

Keywords CFD · Eulerian · cavitation · atomization · validation

1 Introduction

Cavitation is defined as the phase change phenomenon from liquid to vapor due to a static pressure decrease down to the liquid vapor pressure or lower. The decompression of the flow occurs due to flow acceleration (Venturi effect) or flow separation. Thus, vapor bubbles (or vapor cavities) are formed and travel with the flow. They may reach regions with higher pressures, imploding or collapsing (phase-changing back to liquid state) releasing large amount of energy that modifies the flow structure (leading to noise and vibrations) and, if a surface is nearby, eroding it [21]. This can be useful, for instance, for machining thermal-sensitive materials by cavitating waterjet [24]. Unfortunately, cavitation occurs and cannot be avoided in many other applications where its effects are negative, such as fuel injectors [15,41] (field in which cavitation also presents some benefits [1]), hydro-turbines, valves and pumps, ship propellers [16] and even vascular tissue [25]. Therefore, understanding the physics of the cavitation phenomenon is important, but still not completely done [13].

A wide range of both experimental and computational methods have been employed until now to study the cavitation phenomenon. The consulted ones in order to carry out this work are summarized in Table 1. From the experimental point of view, S. Jahangir et al. [18] list many of the existing techniques: high-speed visualization, electrical capacitance tomography, radioactive particle tracking computed tomography, magnetic resonance imaging, impedance tomography systems, and gamma and x-ray imaging (detailed in the work of D. Duke et al. [12]). This last is the one that S. Jahangir et al. [18] used, in combination with high-speed shadowgraphy, to characterize (visualize and quantify) the vapor phase generated by cavitation inside a converging-diverging nozzle. Two different regimes were identified and measured: the re-entrant jet and the bubbly shock. A. Cervone et al. [9] also used high-speed visualization but in combination with surface static pressure measurements to differentiate three cavitation zones around a hydrofoil as function of the cavitation number and temperature: supercavitation, bubble plus cloud cavitation and bubble cavitation. Similar work was done by E. Winklhofer et al. [49] for two-dimensional nozzles. They visualized the cavitating flow by means of diffuse backlight illumination, and at the same time measured the pressure (with a Mach Zehnder interferometer) and velocity (by fluorescence tracing) fields as well as the mass flow rate through the

R. Payri, J. Gimeno, P. Martí-Aldaraví, M. Martínez, "Validation of a three-phase Eulerian CFD model to account for cavitation and spray atomization phenomena", *Journal of the Brazilian Society of Mechanical Sciences and Engineering*, 43(228), pp. 1-15, 2021. DOI:0.1007/s40430-021-02948-z.

nozzle. This work proved that small variations in geometry significantly vary the operating conditions for cavitation to occur. The use of transparent nozzles to study the cavitation phenomenon is a common methodology, and the works of R. Payri et al. [34] and V. Kirsch et al. [20] are good examples of it.

Table 1: Summary of the consulted publications that define the stat of art of research in cavitation phenomenon. Sorted by publication date.

Method	Technique/Model	Application	Phases	Authors and reference
Experimental	DBI	nozzle	diesel+vapor	Winklhofer et al. [49]
Experimental	direct visualization	hydrofoil	water+steam	Cervone et al. [9]
Computational	homogeneous mixture	hydrofoil	water+steam	Morgut et al. [27]
Computational	homogeneous mixture	nozzle	diesel+vapor	Brusiani et al. [7]
Computational	homogeneous mixture	nozzle	diesel+vapor	Salvador et al. [38]
Computational	homogeneous mixture	hydrofoil	water+steam	Yu et al. [51]
Computational	homogeneous mixture	hydrofoil	water+steam	Zhou et al. [53]
Exp./Comp.	visualization/VOF	hydrofoil	water+steam	Arabnejad et al. [2]
Experimental	x-ray/shadowgraphy	nozzle	water+steam	Jahangir et al. [18]

On the other hand, from the computational point of view, there are many cavitation models available in the literature. A. Yu et al. [51] compared the performance of three of them, Zwart, full cavitation and Kunz models, in predicting cavitation structures around a NACA 0015 hydrofoil. It turned out that only Kunz model had accurate prediction for both steady and unsteady states, but did not predict the shearing action of the re-entrant jet on the attached cavity. M. Morgut et al. [27] optimized these three cavitation models so they provided the same accuracy for NACA 66 and NACA 0009 hydrofoils. Schnerr-Sauer cavitation model was employed by M. H. Arabnejad et al. [2] to study shedding mechanisms from leading-edge cavitation over a NACA 0009 hydrofoil. They found out two types of shedding: primary (large-scale cloud cavities) and secondary (detachment of small-scale cavity structures). The Shingal cavitation model was compared to the Homogeneous Relaxation Model (HRM) by F. Brusiani et al. [7] for predicting the experimental results obtained by E. Winklhofer et al. [49] in a two-dimensional nozzle (throttle). Even though both models reproduced the experimental evolution of mass flow as function of pressure drop, Shingal model seemed to better predict the axial and radial distributions of the vapor region. H. Zhou et al. [53] implemented the Schnerr-Sauer, the Zwart and the Bubble-Droplet models in a three-phase solver and used them to simulate the NACA 66 (MOD) hydrofoil as well as a projectile and ventilated cavitating flow with natural cavitation. For them, the Schnerr and Sauer model had the best agreement with the experimental results. A different approach is used by F. J. Salvador et al. [38], who decided for a Homogeneous Equilibrium Model (HEM) to study the flow characteristics of a valve covered orifice (VCO) diesel injector, and found a good agreement between experiments and simulations in mass flow and momentum flux rates.

Most of the consulted experimental and computational works are limited to two phases, the liquid and the vapor. Nevertheless, there are applications where three phases are involved, for example, water, steam and air, or fuel, fuel vapor and air.

R. Payri, J. Gimeno, P. Martí-Aldaraví, M. Martínez, "Validation of a three-phase Eulerian CFD model to account for cavitation and spray atomization phenomena", *Journal of the Brazilian Society of Mechanical Sciences and Engineering*, 43(228), pp. 1-15, 2021. DOI:0.1007/s40430-021-02948-z.

Therefore, the main goal of the present research is the validation of an Eulerian three-phase solver including cavitation phase change phenomenon. To do so, the most accurate and reliable cavitation sub-model, among the existing ones, needs to be identified. During these implementation and identification processes, assumptions and strengths of the tested sub-models are analyzed and put to test, providing directions for future developments and improvements in cavitation modeling. Since the proposed computational model might be applicable for spray simulations, a previously developed and validated spray model [39] in OpenFOAM ® is used as starting point. Three existing cavitation models, the HRM, the Schnerr and Sauer, and the Kunz, based on different physical principles, are added to it and tested. The results of this improved Eulerian model are compared to experiments for three different validation cases: a two-dimensional throttle, the NACA 0015 hydrofoil and a single-hole diesel injector. This last validation case shows the maximum potential of the present model.

2 Methodology

2.1 Model description

The Eulerian Spray Atomization (ESA) model [31] has been modified. A third phase, vapor, has been included together with a phase-change model to account for cavitation. This is an Eulerian homogeneous model, based on the one developed by A. Vallet et al. [44], valid for liquid spray simulations at high Reynolds and Weber numbers when there is small differences in velocity between phases. The dispersion is calculated through a balance equation and the mean size of liquid fragments could be obtained from the mean surface area of the liquid-gas interface per unit volume. However, being the focus of this research the cavitation modeling (and only one of the simulated cases a spray), this part is omitted since it is completely decoupled from the rest of the model.

The transport equation of the liquid mass fraction, Y_l, dispersion is Equation 1, where ρ is the mixture density and $\boldsymbol{U}$ is the velocity vector. The atomization [43] and mixing are considered by the definition of a "turbulent diffusion liquid flux". This diffusion flux is modeled by the Fick's law, being the diffusivity coefficient the ratio between the turbulent viscosity, μ_t, and the Schmidt number, Sc, which is equal to 1 [31]. The term S_v is the source term for phase changing. A second transport equation, Equation 2, is included for the non-condensable gas phase mass fraction, Y_g, similar to the one for the liquid mass fraction.

$$\frac{\partial\left(\rho\, Y_l\right)}{\partial t} + \nabla\cdot\left(\rho\, \boldsymbol{U}\, Y_l\right) - \nabla\cdot\left(\frac{\mu_t}{Sc}\,\nabla Y_l\right) = -\rho\, S_v \tag{1}$$

$$\frac{\partial\left(\rho\, Y_g\right)}{\partial t} + \nabla\cdot\left(\rho\, \boldsymbol{U}\, Y_g\right) - \nabla\cdot\left(\frac{\mu_t}{Sc}\,\nabla Y_g\right) = 0 \tag{2}$$

Regardless the phase-change model employed for obtaining the source term S_v, saturation and critical pressures are two required characteristics. The critical pressure, p_{crit}, is taken as a constant value, whilst the saturation pressure, p_{sat}, is calculated

R. Payri, J. Gimeno, P. Martí-Aldaraví, M. Martínez, "Validation of a three-phase Eulerian CFD model to account for cavitation and spray atomization phenomena", *Journal of the Brazilian Society of Mechanical Sciences and Engineering*, 43(228), pp. 1-15, 2021. DOI:0.1007/s40430-021-02948-z.

from the Antoine Equation 3, where A, B and C are empirical parameters specific of each species.

$$p_{sat} = 10^{A-\frac{B}{C+T}} \tag{3}$$

Once the liquid and non-condensable gas mass fractions are obtained, the density of the three-phase mixture is obtained by an equation of state such as Equation 4. The liquid phase is considered as compressible and its thermodynamical model is the one presented by R. Payri et al. [31], with density, compressibility and enthalpy as function of pressure and temperature by means of polynomial fittings. Both gaseous phases are treated as ideal and perfect gases.

$$\rho = \frac{1}{\frac{Y_l}{\rho_l} + \frac{Y_v}{\rho_g} + \frac{1-Y_l-Y_g}{\rho_v}} \tag{4}$$

As in any other turbulent flow simulation, the turbulence model in cavitating flow cases is crucial especially because of the unsteady nature of the phenomenon. According to previous works [39, 10], the best Reynolds-Averaged Navier-Stokes (RANS) turbulence model to accurately predict the flow field characteristics and obtaining the turbulent viscosity, μ_t, in wall bounded flows (inside the nozzle, where cavitation may occur) as well as in the spray is the SST k-ω, a 2-equation viscosity model [26]. This is because the k-ω model, aggregated with the shear-stress transport (SST) model, provides highly accurate predictions and presents a better performance in adverse pressure gradients and unstable flows than other models such as the standard k-ε [47, 48].

The other balance equations, continuity, momentum and energy, are the common ones used in compressible single-phase solvers, can be easily found in the literature, e.g. the work of H. G. Weller et al. [46], and are presented in Equations 5, 6 (where $\boldsymbol{\tau}$ is the deviatoric stress tensor and the body accelerations forces are neglected) and 7 (in terms of static enthalpy, where κ_{eff} is the effective thermal diffusivity coefficient and K the mean flow kinetic energy), correspondingly.

$$\frac{\partial \rho}{\partial t} + \nabla \cdot (\rho \boldsymbol{U}) = 0 \tag{5}$$

$$\begin{aligned} \frac{\partial (\rho \boldsymbol{U})}{\partial t} + \nabla \cdot (\rho \boldsymbol{U} \boldsymbol{U}) &= -\nabla p + \nabla \cdot \boldsymbol{\tau} \\ \boldsymbol{\tau} &= \mu_{eff} \left(\nabla \boldsymbol{U} + \nabla \boldsymbol{U}^T \right) - \frac{2}{3} \mu_{eff} \nabla \boldsymbol{U} \cdot \boldsymbol{I} \end{aligned} \tag{6}$$

$$\frac{\partial (\rho h)}{\partial t} + \nabla \cdot (\rho \boldsymbol{U} h) - \nabla \cdot \left(\kappa_{eff} \nabla h \right) = -\frac{\partial p}{\partial t} - \frac{\partial K}{\partial t} - \nabla \cdot (\rho \boldsymbol{U} K) + \boldsymbol{\tau} : \nabla \boldsymbol{U} \tag{7}$$

That is not exactly the case for the pressure equation, Equation 8, where a_p and $\boldsymbol{H}(\boldsymbol{U})$ correspondingly stand for the diagonal and off-diagonal contributions of the discretized momentum equation [17]. Following the work of S. K. Rachakonda et al. [35], the dependence of the density on the phases mass fractions needs to be considered in the pressure balance, and the first term of Equation 8 can be written as in Equation 9 through the equation of state of Equation 4. The time derivatives of liquid and non-condensable gas mass fractions are known once their corresponding

R. Payri, J. Gimeno, P. Martí-Aldaraví, M. Martínez, "Validation of a three-phase Eulerian CFD model to account for cavitation and spray atomization phenomena", *Journal of the Brazilian Society of Mechanical Sciences and Engineering*, 43(228), pp. 1-15, 2021. DOI:0.1007/s40430-021-02948-z.

transport equations are solved. The compressiblity of the mixture, Ψ, is defined in Equation 10 based on the isothermal acoustic speed of the two-phase flow in terms of each phase volume fraction, $X_i = Y_i \cdot \rho / \rho_i$, $i \in \{l, v, g\}$ [45].

$$\frac{\partial \rho}{\partial t} + \nabla \cdot \left(\frac{\boldsymbol{H}(\boldsymbol{U})}{a_p} \right) - \nabla \cdot \left(\frac{1}{a_p} \nabla p \right) = 0 \tag{8}$$

$$\begin{aligned} \frac{\partial \rho}{\partial t} &= \frac{\partial \rho}{\partial p}\frac{\partial p}{\partial t} + \frac{\partial \rho}{\partial Y_l}\frac{\partial Y_l}{\partial t} + \frac{\partial \rho}{\partial Y_g}\frac{\partial Y_g}{\partial t} = \\ &= \Psi \frac{\partial p}{\partial t} - \rho^2 \left(\frac{1}{\rho_l} - \frac{1}{\rho_v} \right) \frac{\partial Y_l}{\partial t} - \rho^2 \left(\frac{1}{\rho_g} - \frac{1}{\rho_v} \right) \frac{\partial Y_g}{\partial t} \end{aligned} \tag{9}$$

$$\Psi = \frac{1}{a^2} = \rho \left(\frac{X_l}{\rho_l}\Psi_l + \frac{X_g}{\rho_g}\Psi_g + \frac{1 - X_l - X_g}{\rho_v}\Psi_v \right) \tag{10}$$

OpenFOAM 4.1.0 ® is the finite volume Computational Fluid Dynamics (CFD) code for this study because it is open source, so new submodels and solvers are easy to develop and test, as done in previous works [31]. Transport equations are solved within a PIMPLE (combination of Pressure Implicity with Splitting Operators -PISO, 4 iterations- and Semi-Implicity Method for Pressure-Linked Equations -SIMPLE, 2 iterations-) loop, which increases computational cost but ensures stability and accuracy. For all cases of this investigation, upwind discretization schemes are used to minimize the computational cost with relatively low computational error. A first-order implicit Euler scheme is selected for the time discretization. PBiCG (Preconditioned Bi-Conjugate Gradient) solver with DILU (Diagonal Incomplete LU) preconditioner is used for all variables but the pressure, which is solved by PCG (Preconditioned Conjugate Gradient) solver with DIC (Diagoanal Incomplete Cholesky) preconditioner. A relaxation factor of 0.3 is used for the pressure, a factor of 0.7 is set for the density, and the rest of variables are solved without relaxation.

2.2 Homogeneous Relaxation Model (HRM) for cavitation

The HRM defines the phase change source term, S_v, with Equation 11. As explained by Z. Bilicki et al. [6], this equation describes how the local and instantaneous vapor mass fraction ("quality"), Y_v, tends toward its local unconstrained-equilibrium value $\bar{Y}_{v,eq}(p,T)$. In order to account for non-equilibrium effects, it is assumed that the composition parameter Y_v does not adjust itselft to the equilibrium value $\bar{Y}_{v,eq}$ introducing a finite relaxation time, θ. As shown in Equation 12 [35], this relaxation time depends on the local instantaneous vapor volume fraction, X_v, and a non-dimensional pressure, ψ, defined in Equation 13.

$$S_v = \frac{\bar{Y}_{v,eq} - Y_v}{\theta} \tag{11}$$

$$\theta = \theta_0 X_v^{-0.54} \psi^{-1.76} \tag{12}$$

$$\psi = \left| \frac{p_{sat} - p}{p_{crit} - p_{sat}} \right| \tag{13}$$

R. Payri, J. Gimeno, P. Martí-Aldaraví, M. Martínez, "Validation of a three-phase Eulerian CFD model to account for cavitation and spray atomization phenomena", *Journal of the Brazilian Society of Mechanical Sciences and Engineering*, 43(228), pp. 1-15, 2021. DOI:0.1007/s40430-021-02948-z.

K. Saha et al. [37] performed a complete parametric study of the constant θ_0 value and the exponents in Equation 12 for a gasoline direct injection application. The parameter θ_0 was varied from 10^{-6} to 10^{-8}, resulting that the order of 10^{-7} s was reasonable. In this case, a value of $\theta_0 = 3.84 \cdot 10^{-8}$ s is selected for wall bounded flows and a value of $\theta_0 = 3.84 \cdot 10^{-6}$ s for free flow cases. In both situations an order of magnitude different than the one used by other researchers [35]. Regarding the exponents, they were also varied in a reasonable range, leading to the conclusion that values used by other researchers and shown in Equation 12 allow accurate prediciction of both cavitation and flash-boiling phenomena.

The equilibrium vapor mass fraction, $\bar{Y}_{v,eq}$, corresponds to the thermodynamic quality of Equation 14 [4, 11], where h is the local and instantaneous enthalpy of the fluid and $h_{l,sat}$ and $h_{v,sat}$ are the saturated liquid and vapor enthalpies, respectively, calculated as function of temperature at the saturation pressure, $h_{i,sat} = h_i(p_{sat}, T)$. In the present study, this equilibrium vapor quality is limited to the saturated region, $0 \leq \bar{Y}_{v,eq} \leq 1$, dismissing the subcooled ($\bar{Y}_{v,eq} < 0$) and the superheated ($\bar{Y}_{v,eq} > 1$) conditions.

$$\bar{Y}_{v,eq}(p,T) = \frac{h_l(p,T) - h_{l,sat}}{h_{v,sat} - h_{l,sat}} \tag{14}$$

Following the comments from K. Saha et al. [37], for cases where there is no vapor or where local pressure is equal to the saturation pressure, the source term in Equation 11 tends to infinity because the relaxation time θ becomes zero. To negate this issue, $X_{v,min} = 10^{-4}$ and $\psi_{min} = 10^{-12}$ are used as thresholds when computing the relaxation time. Other possible solution for the absence of vapor issue is the inclusion of non-condensable gases within the liquid phase [4]. Being true for liquid fuels, this assumption might not be accurate for all the three validation cases of this investigation.

2.3 Schnerr and Sauer cavitation model

Originally developed by G. Schnerr and J. Sauer [40], this model is based on the approach that the liquid fluid contains a large number of spherical gas bubbles (being eiter non-condensable gases or vapor phase). The mass exchange rate is then based on a simplified model for bubble growth, based on the Rayleight-Plesset equation, which is solved neglecting second order terms and the surface tension and generalized to include condensation [54], yields to Equation 15. It should therefore account for non-equilibrium effects.

$$S_v = -\frac{\rho_v \rho_l}{\rho^2} X_l X_v \frac{3}{R_b} \operatorname{sign}(p - p_{sat}) \sqrt{\frac{2}{3} \frac{|p - p_{sat}|}{\rho_l}} \tag{15}$$

The concentration of the cavitation nuclei, n_0, and therefore the radius of the vapor bubbles, R_b (Equation 16), depend on many factors. According to G. Cazzoli et al. [8], these are the temperature, the difference between local pressure and the vapor pressure and the purity of the fluid. The same authors suggest a constant value of $n_0 = 10^{13}\,\mathrm{m}^{-3}$, which is employed in this investigation for wall bounded flows.

R. Payri, J. Gimeno, P. Martí-Aldaraví, M. Martínez, "Validation of a three-phase Eulerian CFD model to account for cavitation and spray atomization phenomena", *Journal of the Brazilian Society of Mechanical Sciences and Engineering*, 43(228), pp. 1-15, 2021. DOI:0.1007/s40430-021-02948-z.

However, a value of $n_0 = 5 \cdot 10^8\,\mathrm{m}^{-3}$, several orders of magnitude lower, is needed for the free flow case to get convergence of the case and realistic results.

$$R_b = \left(\frac{X_v}{X_l} \frac{1}{\frac{4}{3}\pi n_0} \right)^{\frac{1}{3}} \tag{16}$$

To avoid numerical issues where there is no vapor or no liquid, minimum thresholds of $X_{v,min} = 10^{-15}$, $X_{l,min} = 10^{-9}$ and $R_{b,min} = 10^{-9}\,\mathrm{m}$ are utilized in Equations 15 and 16, as done for the relaxation time of the HRM.

2.4 Kunz cavitation model

Unlike previous models, the mass transfer here is based on different strategies for vaporization and condensation. As explained in the work of R. F. Kunz et al. [22], the vaporization of the liquid phase is proportional to the liquid volume fraction and the amount by which the pressure is below the vapor pressure, as shown in Equation 17, where U_∞ is the characteristic flow velocity. On the other hand, the condensation of vapor into liquid is modeled with a simplified form of the Ginzburg-Landau potential, the third order polynomial function of the vapor volume fraction of Equation 18 (the liquid volume fraction can be written as $X_l = 1 - X_g - X_v$), which is non-dimensionalized with respect to a mean flow time scale, t_∞.

$$\dot{m}_{vap} = C_{prod}\,\rho_v X_l \frac{\min(0, p - p_{sat})}{\frac{1}{2}\rho_l U_\infty^2 t_\infty} \tag{17}$$

$$\dot{m}_{con} = C_{dest}\,\rho_v X_l \frac{X_v^2}{t_\infty} \tag{18}$$

Thus, the specific mass transfer source term is computed as in Equation 19. In this model, vaporization phenomenon is restricted to the zones where pressure is below the saturation value and there is some liquid to vaporize, while condensation occurs independently of the pressure in the regions with vapor phase, having a maximum in condensation rate at $X_v = 1/3$.

$$S_v = \frac{\dot{m}_{con} - \dot{m}_{vap}}{\rho} \tag{19}$$

In Equation 17 and Equation 18 there are two empirical constants whose values change from one investigation to another. For instance, R. F. Kunz et al. [23] use $C_{prod} = 0.2$ and $C_{dest} = 0.2$, whilst R. F. Kunz et al. [22] employ $C_{prod} = 100$ and $C_{dest} = 100$, and A. Yu et al. [51] take $C_{prod} = 455$ and $C_{dest} = 4100$. In order to minimize this uncertainty, and in a similar way of K. Saha et al. [37], H. Zhou et al. [52] performed a sensitivity study and a sequential optimization of these two constants for a 2D airfoil and a series of hemispherical head-forms, leading to the following optimized values: $C_{prod} = 3323$ and $C_{dest} = 4328$. Following their work, these are the values employed for all cases of the present investigation.

3 Validation cases setup

3.1 2D throttle

The first validation case corresponds to the two-dimensional throttle arrangement developed and tested by E. Winklhofer et al. [49]. It has been previously used as validation case by other researches, for example, F. Brusiani et al. [7]. Even though they tested three different geometries with three different contraction levels, only one of them with a contraction of 5%, named "throttle U", is selected for validation purposes. The geometry consists of a channel with an inlet height of $H_i = 301\,\mu$m, an outlet height of $H_o = 284\,\mu$m and an inlet fillet radius of $20\,\mu$m, as shown in Figure 1. Two plenums are placed upstream ($15H_1 \times 15H_1$) and downstream ($65H_1 \times 30H_1$) the channel to avoid any effect of the boundary conditions on the region of interest.

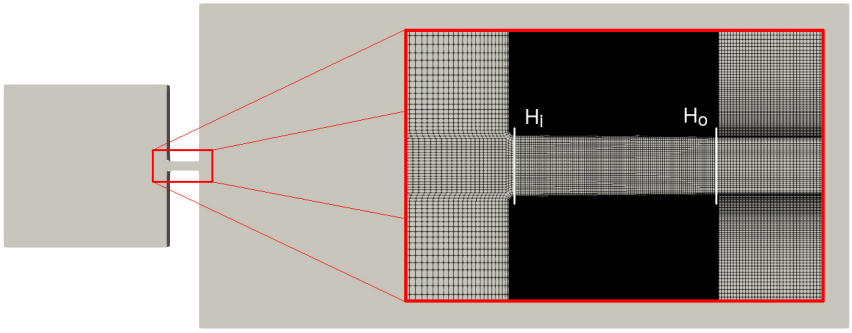

Fig. 1: Geometry and mesh of the "throttle U" validation case.

The fluid employed in the experiments was standard diesel fuel. However, a single-component surrogate, n-dodecane, is chosen as the working fluid for the simulations to enable a complete knowledge of the thermophysical properties of the fluid [31]. This is a common strategy in the engine research community [3].

The stagnation pressure is fixed at the inlet, on the left hand side in Figure 1, equal to 10 MPa in all simulations. The fluid temperature at inlet is also constant and equal to 300 K. The static pressure is set at the outlet, on the right hand side in Figure 1, its value varying from 1.5 MPa to 8 MPa depending on the desired pressure drop through the throttle. The rest of the boundaries are non-slip adiabatic walls (in accordance to the findings of R. Payri et al. [31]).

A structured mesh with quadrilateral cells is employed for this case and also for the other two. After a mesh sensitivity analysis performed with the HRM for cavitation and a pressure drop of 8.5 MPa, the selected mesh is the one with 119924 elements, being part of it shown in Figure 1, because it represents the best compromise between computational cost and accuracy. The analysis is summarized in Table 2, where the mass flow rate at the outlet section, $\dot{m}$, is the comparison parameter.

R. Payri, J. Gimeno, P. Martí-Aldaraví, M. Martínez, "Validation of a three-phase Eulerian CFD model to account for cavitation and spray atomization phenomena", *Journal of the Brazilian Society of Mechanical Sciences and Engineering*, 43(228), pp. 1-15, 2021. DOI:0.1007/s40430-021-02948-z.

Table 2: Results of the mesh sensitivity analysis of the “throttle U” validation case.

Cell count	Min. size	Max. size	$\dot{m}$ at outlet	Variation
53068	2.1 µm	235 µm	8.081 g/s	-
119924	1.5 µm	160 µm	7.993 g/s	1.10%
270337	1.0 µm	105 µm	7.942 g/s	0.64%

3.2 NACA 0015 airfoil

The flow around a NACA 0015 hydrofoil represents the second validation case. It is a common basic geometry to study cavitation appearance utilized by, among others, G. Schnerr and J. Sauer [40] and A. Yu et al.[51]. Particularly, experiments and simulations of A. Yu et al. [51] are reproduced in this work. The chord length of the airfoil is $\bar{c} = 0.07$ m, placed inside the water flow with an angle of attack of $\alpha = 6°$. The two-dimensional computational domain, shown in Figure 2, extends to $20 \times \bar{c}$ downstream and $10 \times \bar{c}$ in the other directions.

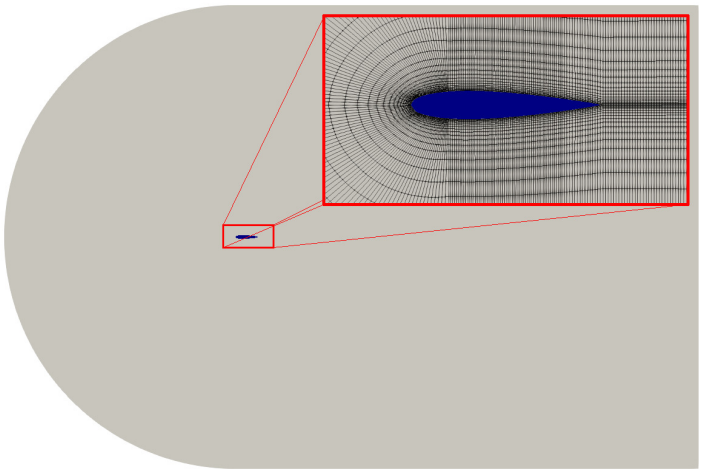

Fig. 2: Geometry and mesh of the “NACA 0015” validation case.

The working fluid for this case is water. All of the required thermophysical properties (of both liquid and vapor phases) are obtained from the NIST database [28]. The surface of the airfoil is modeled as non-slip adiabatic wall [31]. The farthest section downstream is a pressure outlet boundary condition, and the rest of the limits of the domain are considered free-stream. Pressure and temperature at outlet and free-stream boundaries are 31 325 Pascal and 298 K, and the free-stream velocity is set to 7.2 m/s with a turbulent intensity of 5% and a turbulent length scale of 10% of $\bar{c}$. The simulated conditions correspond to a Reynolds number of $Re = 5.652 \cdot 10^5$, in other words, to turbulent flow around the NACA 0015 hydrofoil.

R. Payri, J. Gimeno, P. Martí-Aldaraví, M. Martínez, “Validation of a three-phase Eulerian CFD model to account for cavitation and spray atomization phenomena”, *Journal of the Brazilian Society of Mechanical Sciences and Engineering*, 43(228), pp. 1-15, 2021. DOI:0.1007/s40430-021-02948-z.

Table 3 depicts the mesh sensitiviy analysis performed in this case. The elements with the minimum cell size are the ones next to the airfoil, whilst the largest elements are located far downstream. The comparison parameter is the lift coefficient of the airfoil, c_l defined in Equation 20, being L the 2D force perpendicular to the free-stream velocity. The best of the tested grids is the one with 147888 elements.

$$c_l = \frac{L}{\frac{1}{2}\rho_l U_\infty^2 \bar{c}} \tag{20}$$

Table 3: Results of the mesh sensitivity analysis of the "NACA 0015" validation case.

Cell count	Min. size	Max. size	c_l	Variation
29120	395 µm	11.05 mm	0.4613	-
65520	265 µm	7.41 mm	0.4493	2.67%
147888	180 µm	4.92 mm	0.4784	6.08%
331344	120 µm	3.25 mm	0.4768	0.33%

3.3 ECN Spray C

The third and last validation case is one of the diesel injectors of the Engine Combustion Network (ECN) [42], concretely the one named "Spray C" [30]. It is a large-nozzle single-hole injector from Bosch (Bosch 3-22). Its hole is cylindrical (k-factor $= (D_{in} - D_o)/10$ equal to zero) with nominal outlet diameter of $D_o = 200\,\mu\text{m}$ and a 5% of hydro-erosion to relatively smooth the contours of the orifice. The geometry of the nozzle has been obtained by x-ray tomography [19]. Following one of the methodologies presented by M. Battistoni et al. [5], a two-dimensional axisymmetric (wedge) version of it, depicted in Figure 3, has been built for this investigation. A plenum ($12\,\text{mm} \times 6\,\text{mm}$) has been attached to consider the ambient conditions. This is the case where the three phases are present because the discharge volume is filled with N_2 (non-reactive atmosphere similar to air).

The working fluid is again n-dodecane, as in the "Throttle U" validation case, the standard surrogate at ECN for diesel. The inlet of the nozzle is represented with a time-varying velocity condition and constant temperature equal to 343 K [39]. The time resolved value of the velocity is obtained from the experimental measurements of mass flow rate [30], at 150 MPa of injection pressure. The turbulent intensity at the inlet is equal to 5% of the imposed velocity and the turbulent length scale is 10% of the orifice outlet diameter. The plenum, on the right hand end, is a non-reflective or wave transmissive boundary condition, with a pressure value that gives an ambient density of $22.8\,\text{kg/m}^3$ at a temperature of 303 K (nominal ECN conditions). The rest of the boundaries are non-slip adiabatic walls [31]. For the initialization, the nozzle is considered to be filled (up to the orifice outlet) with stagnated fuel at injection temperature [32].

R. Payri, J. Gimeno, P. Martí-Aldaraví, M. Martínez, "Validation of a three-phase Eulerian CFD model to account for cavitation and spray atomization phenomena", *Journal of the Brazilian Society of Mechanical Sciences and Engineering*, 43(228), pp. 1-15, 2021. DOI:0.1007/s40430-021-02948-z.

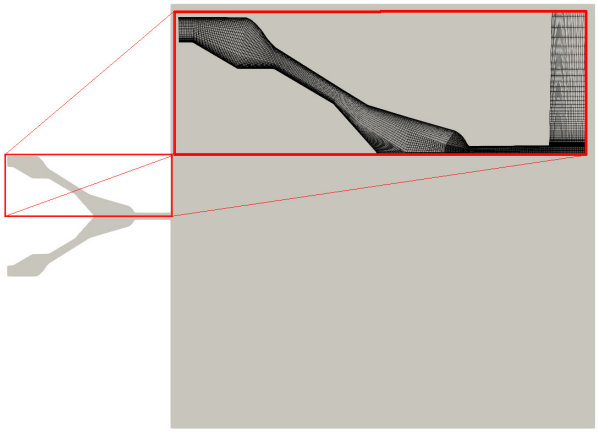

Fig. 3: Geometry of the "Spray C" validation case.

The mesh sensitivity analysis of this case, carried out also with the HRM, is summarized in Table 4. The minimum cell size is located at the orifice outlet section, next to the wall. The steady state mass flow rate at the orifice outlet, $\dot{m}$, is again used as comparison parameter. In this case, the selected mesh (shown in Figure 3) is the one with 29524 cells.

Table 4: Results of the mesh sensitivity analysis of the "Spray C" validation case.

Cell count	Min. size	Max. size	$\dot{m}$ at outlet	Variation
16761	1.5 µm	718 µm	12.398 g/s	-
29524	1 µm	489 µm	11.458 g/s	8.2%
62072	0.7 µm	330 µm	11.780 g/s	2.7%
150092	0.45 µm	220 µm	11.419 g/s	3.2%

4 Results

4.1 2D throttle

Steady state mass flow through the throttle as function of the pressure drop is depicted in Figure 4a, where simulation data is compared to experiments from E. Winklhofer et al. [49]. Results of the three tested cavitation models are almost the same, and similar to experimental values, being the mass flow under non-cavitating conditions proportional to the square root of pressure drop. According to E. Winklhofer et al. [49], cavitation starts around a pressure drop of 6 MPa, having a small effect on the mass flow trend. However, the amount of vapor in the simulations is negligible for pressure drops of 7.5 MPa and below. A delay in the onset of cavitation is predicted by all models. Another relevant difference is the slight over-prediction (about a 2.3%)

R. Payri, J. Gimeno, P. Martí-Aldaraví, M. Martínez, "Validation of a three-phase Eulerian CFD model to account for cavitation and spray atomization phenomena", *Journal of the Brazilian Society of Mechanical Sciences and Engineering*, 43(228), pp. 1-15, 2021. DOI:0.1007/s40430-021-02948-z.

of the chocked mass flow value. These two differences can be attributed to the difference in the saturation pressure value characterizing the experimental diesel and the surrogate adopted for these simulations (which has about 4 times higher saturation pressure than standard diesel) [7].

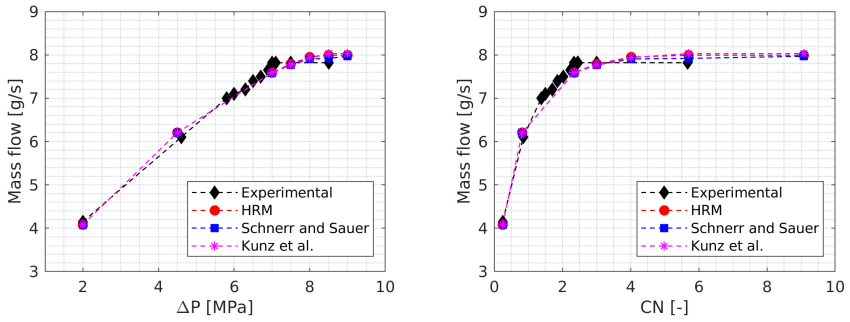

(a) Mass flow vs. pressure drop.

(b) Mass flow vs. cavitation number.

Fig. 4: Hydraulic behavior of the "throttle U" validation case.

Mass flow is plotted also versus the cavitation number in Figure 4b. Cavitation inception number (CN) is defined in Equation 21, being the first definition the one used in wall bounded pressure driven flows whilst its equivalent, the second definition, is used in free flow situations. In nozzles, the cavitation number at which the mass flow is 99% of the chocked value is known as the critical cavitation number (CCN). E. Winklhofer et al. [49] provided a value of $CCN = 2.33$ for this case, and proved that it depends on the geometry. Nonetheless, based on the results of F. Brusiani et al. [7] and the ones presented here, it can be assumed that it also depends on the working fluid. The values obtained by F. Brusiani et al. [7] are $CCN = 2.4 - 2.5$, but for the present study they would be between 3 and 4.

$$CN = \frac{p_{in} - p_{out}}{p_{out} - p_{sat}} = \frac{\frac{1}{2}\rho_l U_\infty^2}{p_\infty - p_{sat}} \tag{21}$$

These results prove that the correlation of the simulations with experiments is not perfect because the working fluid could not be exactly the same. Nevertheless, additional comparisons provide interesting results. Figure 5 shows the velocity profiles at two different sections of the throttle, near the inlet. As shown in Figure 5a, for the section closest to the throttle inlet, a velocity peak is found in the experiments close to the walls of the throttle. According to the explanation of F. Brusiani et al. [7], vapor has lower density than liquid, and so, zones where there is vapor suffer from an increase in velocity by conservation of momentum. This behavior is not captured by the simulations because of three reasons. The first one is the assumption of homogeneous flow, which implies infinite momentum transfer between phases (clearly overestimating it). This leads to the second reason, the assumption of zero slip velocity between

R. Payri, J. Gimeno, P. Martí-Aldaraví, M. Martínez, "Validation of a three-phase Eulerian CFD model to account for cavitation and spray atomization phenomena", *Journal of the Brazilian Society of Mechanical Sciences and Engineering*, 43(228), pp. 1-15, 2021. DOI:0.1007/s40430-021-02948-z.

phases, it might not be true when part of the nozzle is fully occupied by vapor. And the third one is that the selected turbulence model may have high energy dissipation rate near the wall, or may not account for all the compressibility effects present in multiphase flow [10]. Far from walls, the velocity is almost constant with a minimum in the centerline. This trend is well captured by the simulations, being the differences in the velocity values explained by the different fluid properties of standard diesel and n-dodecane (which has slightly lower density). Further downstream, in a section in the main part of the flow contraction, the velocity profiles re-arranges itself and the maximum can be found in the centerline as shown in Figure 5b. Nonetheless, experiments under chocked flow conditions show also maximum velocities near the liquid-gas interphase. Behavior which again is not reproduced by the simulations. Nevertheless, the current accuracy in the velocity profiles is similar to the one reported in the literature [7].

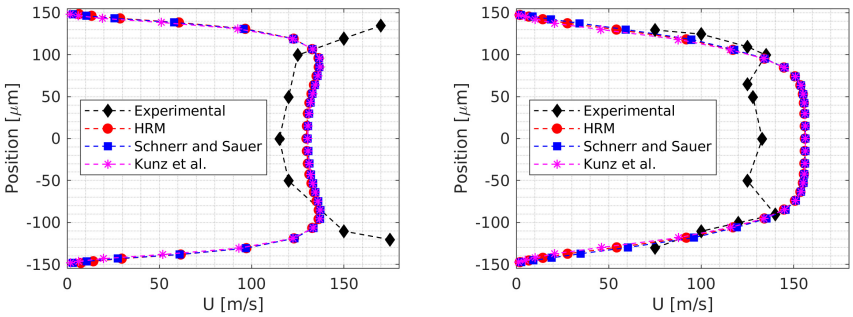

(a) At 53 µm from the inlet.

(b) At 170 µm from the inlet.

Fig. 5: Velocity profiles of the "throttle U" validation case with a pressure drop of 8.5 MPa.

The deattached zone as well as the area occupied by vapor seem to be well reproduced by the simulations in Figure 5. For better visualization of it, the steady state liquid volume fraction contours at three different values of pressure drop are depicted in Figure 6, including the experimental results from E. Winklhofer et al. [49]. Two of the pressure drop values of the experimental results do not coincide with the simulated ones because, as it has been previously mentioned, the onset of cavitation predicted by the models is delayed. While in the experiments cavitation is firstly observed at pressure drops of 6.0 MPa, simulations do not predict noticeable vapor until the pressure drop reaches at least 7.5-8.0 MPa. Therefore, a direct comparison between experiments and simulations is not possible. For operating conditions beyond critical cavitation, all models predict that the axial extension of vapor covers up to the outlet, but none of them accurately predict the vapor expansion towards the axis. Although this inaccuracy has been already reported by F. Brusiani et al. [7], who linked it to the different way of obtaining the countour, it seems that all models underpredict the area occupied by the vapor phase downstream, close to the outlet section.

R. Payri, J. Gimeno, P. Martí-Aldaraví, M. Martínez, "Validation of a three-phase Eulerian CFD model to account for cavitation and spray atomization phenomena", *Journal of the Brazilian Society of Mechanical Sciences and Engineering*, 43(228), pp. 1-15, 2021. DOI:0.1007/s40430-021-02948-z.

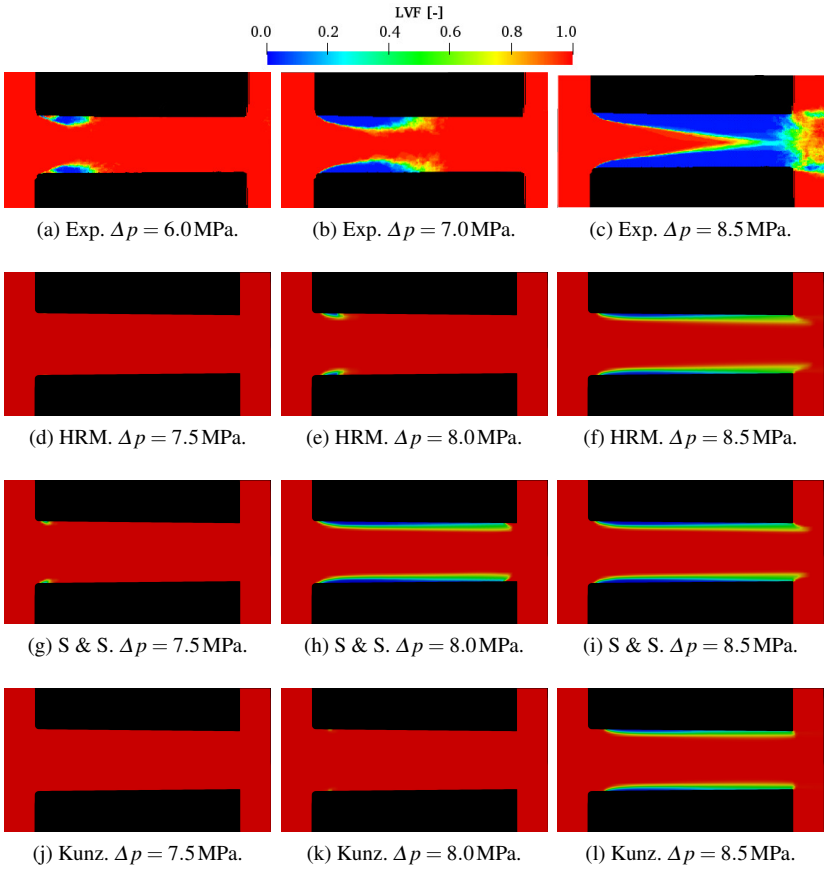

(a) Exp. $\Delta p = 6.0\,\mathrm{MPa}$. (b) Exp. $\Delta p = 7.0\,\mathrm{MPa}$. (c) Exp. $\Delta p = 8.5\,\mathrm{MPa}$.

(d) HRM. $\Delta p = 7.5\,\mathrm{MPa}$. (e) HRM. $\Delta p = 8.0\,\mathrm{MPa}$. (f) HRM. $\Delta p = 8.5\,\mathrm{MPa}$.

(g) S & S. $\Delta p = 7.5\,\mathrm{MPa}$. (h) S & S. $\Delta p = 8.0\,\mathrm{MPa}$. (i) S & S. $\Delta p = 8.5\,\mathrm{MPa}$.

(j) Kunz. $\Delta p = 7.5\,\mathrm{MPa}$. (k) Kunz. $\Delta p = 8.0\,\mathrm{MPa}$. (l) Kunz. $\Delta p = 8.5\,\mathrm{MPa}$.

Fig. 6: Liquid volume fraction contours of the "throttle U" validation case.

Once again, in this case, the main difference between the three tested cavitation models is not the vapor distribution but the onset of cavitation. As observed in Figure 6, for the pressure drop of $\Delta p = 8.5\,\mathrm{MPa}$, liquid volume fraction distributions of Figures 6f, 6i and 6l are very similar. The Schnerr and Sauer model is the only one that shows significant amount of vapor with a pressure drop of $\Delta p = 7.5\,\mathrm{MPa}$. The stabilization of vapor cavities for the same pressure drop, shown in Figures 6e, 6h and 6k, is also different. For the Schnerr and Sauer model it almost reaches the outlet whilst for the HRM and the Kunz the vapor phase is confined in a region close to the throttle inlet, although the Kunz model barely generates vapor under this pressure conditions. This behavior is related to the assumptions made by each model. For instance, the Schnerr and Sauer accepts that the liquid contains a large number of gas bubbles which act as initiators of cavitation, so cavitation appears earlier than in the other models.

R. Payri, J. Gimeno, P. Martí-Aldaraví, M. Martínez, "Validation of a three-phase Eulerian CFD model to account for cavitation and spray atomization phenomena", *Journal of the Brazilian Society of Mechanical Sciences and Engineering*, 43(228), pp. 1-15, 2021. DOI:0.1007/s40430-021-02948-z.

4.2 NACA 0015 airfoil

Experimental data from A. Yu et al. [50], in terms of wall pressure coefficient as defined in Equation 22, is compared to current simulation data of the three different cavitation models in Figure 7. Both suction and pressure sides of the hydrofoil are plotted. Unfortunately, experimental information is available only for the suction side until approximately $x/\bar{c} = 0.55$, area where cavitation is expected to occur. The observed low, below saturation pressure (high "$-c_p$" values), and almost constant pressure corresponds to the presence of vapor phase, which according to A. Yu et al. [50,51] extends to approximately $x/\bar{c} = 0.4 - 0.45$. After the sharp pressure coefficient rise, predicted only by HRM and Schnerr and Sauer models, the flow is compound of only liquid water. From there, the pressure increases gently, which means a small pressure gradient over that part of the suction side, equally resolved by all the cavitation models as expected.

$$c_p = \frac{p - p_\infty}{\frac{1}{2}\rho_l U_\infty^2} \tag{22}$$

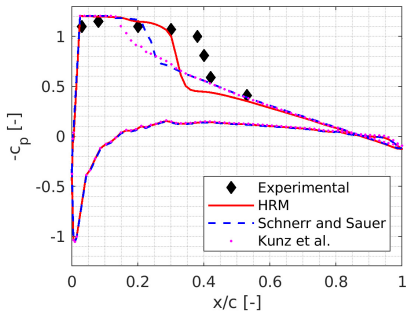

Fig. 7: Wall pressure coefficient of the "NACA 0015" validation case.

As clearly shown in Figure 7, the HRM is the model that best reproduces the experimental results. The pressure rise which denotes the end of the cavitation region is found at approximately $x/\bar{c} = 0.3 - 0.35$, whilst for the Schnerr and Sauer it is located at around $x/\bar{c} = 0.2 - 0.25$. The magnitude of the pressure change is very well reproduced by the HRM, while it is about half of the experimental one for the Schnerr and Sauer model. The Kunz model, which for A. Yu et al. [51] provided very good accuracy, does not present vapor phase in the vecinity of the leading edge of the airfoil, and that is why from almost $x/\bar{c} = 0.1$ the pressure gradient on the suction side is small. A. Yu et al. [51] obtained this kind of behavior not for the Kunz but for the full cavitaion model (FCM), not included in this investigation because, for them, it was inconsistent with the experimental results. On the other hand, the predicted values for the wall pressure coefficient along the pressure side of the hydrofoil are obviously the same regardless the cavitation model. No phase change is expected on that side because the local pressure values, even though they decrease for large part of

R. Payri, J. Gimeno, P. Martí-Aldaraví, M. Martínez, "Validation of a three-phase Eulerian CFD model to account for cavitation and spray atomization phenomena", *Journal of the Brazilian Society of Mechanical Sciences and Engineering*, 43(228), pp. 1-15, 2021. DOI:0.1007/s40430-021-02948-z.

the hydrofoil length ($c_p < 0$ from approximately $x/\bar{c} = 0.15$), do not reach the water saturation pressure.

Continuing with the comparison with experiments, Figure 8 shows the liquid volume fraction contours around the hydrofoil. They correspond to a cloud cavitation regime, as expected for this case with $CN = 0.856$. Figure 8a was obtained by A. Yu et al. [51] by luminescence, and allows to qualitatively locate the cavitation bubbles. As previously commented, the cavitation model that provides results closer to experiments is the HRM (Figure 8b). Even though, the area occupied by the vapor phase is underpredicted, as happened in the previous "throttle U" validation case. The Schnerr and Sauer (Figure 8c) reports even smaller size of cavities as well as lower amount of vapor. And Kunz model (Figure 8d) barely generates vapor, being 0.917 the minimum value of the liquid volume fraction found over the suction side of the airfoil.

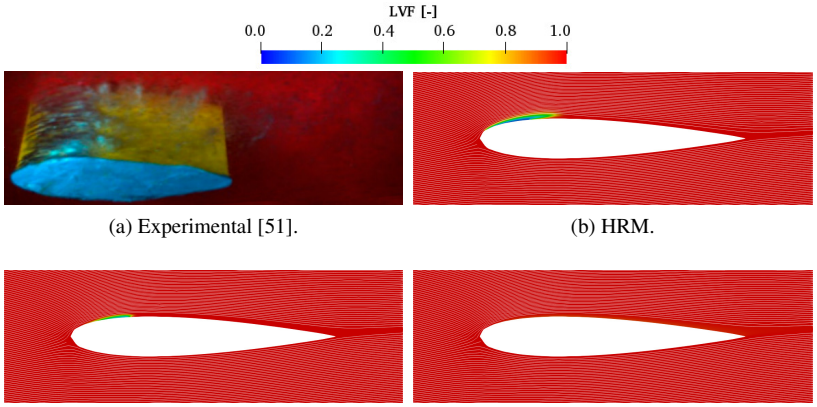

(a) Experimental [51].

(b) HRM.

(c) Schnerr and Sauer.

(d) Kunz.

Fig. 8: Liquid volume fraction contours of the "NACA 0015" validation case. In the countours from CFD simulations, streamlines are also shown.

Two possible sources of uncertainties that could explain the differences observed between experiments and simulations have been identified. The first one is the unsteady nature of the cavitation phenomenon [49–51]. Thus, using a single experimental snapshot as in Figure 8 or a pressure distribution without specifying the experimental variability as in Figure 7 for comparison may lead to not fully substantiated conclusions. From the computational point of view, running steady-state simulations such as the ones reported here could lead to a loss of accuracy. The second one is related to turbulence. As observed in Figures 8b and 8c, vapor cavities location is closely related to flow separation regions. Therefore, a RANS turbulence model capable of predicting flow detachment and reattachment is needed. For S. Obeid et al. [29], that was the Realizable k-ε instead of the SST k-ω employed in the current simulations. The preformance of these two turbulence models for this particular case is very similar, as shown in Figures 9 and 10, where results of a simulation with the

R. Payri, J. Gimeno, P. Martí-Aldaraví, M. Martínez, "Validation of a three-phase Eulerian CFD model to account for cavitation and spray atomization phenomena", *Journal of the Brazilian Society of Mechanical Sciences and Engineering*, 43(228), pp. 1-15, 2021. DOI:0.1007/s40430-021-02948-z.

Standard k-ε model are also included. Realizable k-ε and SST k-ω models predict almost the same separation, with a peak of turbulent kinetic energy in the area of vapor condensation and flow reattachment, and so cavitation areas over the suction side of the hydrofoil, whilst the Standard k-ε does not predict flow separation at all, so phase-change does not occur. This is because the Standard k-ε predicts higher intensity levels (directly related to the turbulent kinetic energy) which allow the boundary layer to remain attached (at $\alpha = 6°$).

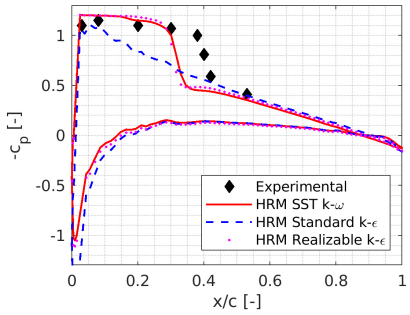

Fig. 9: Wall pressure coefficient of the "NACA 0015" validation case for different RANS turbulence closure models.

4.3 ECN Spray C

Nozzle discharge, velocity and area coefficients, defined in Equation 23 (where $\dot{m}$ and $\dot{M}$ represent the mass flow and momentum flux at the outlet, respectively), together with the experimental results from R. Payri et al. [30], are listed in Table 5. The cavitation model that predicts values closer to experiments is the HRM, and the one with lowest accuracy is the Kunz model. The three of them underpredict the area occupied by the vapor phase, as demonstrated by the overprediction in area coefficient. This result is consistent with the flow structure obtained in the simulations for the "throttle U" validation case, shown in Figure 6 and the work of F. Brusiani et al. [7], with the vapor occupying lower area than in the experimental observations.

$$\begin{aligned} C_d &= \frac{\dot{m}}{A_o \sqrt{2\rho_l \Delta p}} = C_a C_v \\ C_M &= \frac{\dot{M}}{2A_o \Delta p} = C_a C_v^2 \end{aligned} \tag{23}$$

Differences in cavitation prediction between the tested models can be visualized in the liquid volume fraction contours of Figure 11. A length of $10 \times D_o$ of the discharge volume is shown together with nozzle. The black line represents the zone where the vapor volume fraction is higher than 0.1%. Cavitation starts at the nozzle

R. Payri, J. Gimeno, P. Martí-Aldaraví, M. Martínez, "Validation of a three-phase Eulerian CFD model to account for cavitation and spray atomization phenomena", *Journal of the Brazilian Society of Mechanical Sciences and Engineering*, 43(228), pp. 1-15, 2021. DOI:0.1007/s40430-021-02948-z.

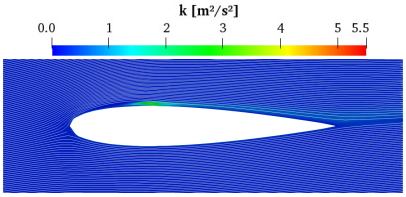

(a) HRM SST k-ω.

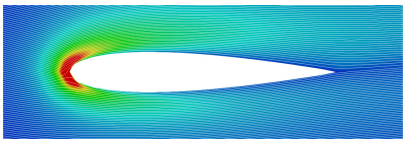

(b) HRM Standard k-ε.

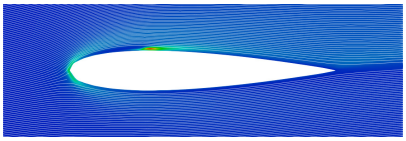

(c) HRM Realizable k-ε.

Fig. 10: Turbulent kinetic energy contours of the "NACA 0015" validation case for different RANS turbulence closure models. Streamlines are also shown.

Table 5: Nozzle flow coefficients of the "Spray C" validation case.

	C_d	C_M	C_v	C_a
Experimental	0.631	0.574	0.910	0.693
HRM	0.680	0.609	0.895	0.759
Schnerr and Sauer	0.708	0.614	0.867	0.817
Kunz	0.726	0.610	0.840	0.864

inlet and extends for the complete orifice length because the cavitation number of this case ($CN = 74.3$) is far beyond the critical cavitation number, plus the orifice is not designed to avoid cavitation (it is straight with low grade of hydroerosion). In fact, HRM shows vapor cavities outside the nozzle, which according to the other two models, collapse just after exiting the nozzle. This implies a small increase in the spray cone angle (defined next, see Table 6 for its results). Unfortunately, additional to the hydraulic characterization already presented in Table 5 there is no more experimental data related to the nozzle flow or the near-field spray to validate these results, being perhaps the USAXS [5] the only technique capable of obtaining extra relevant information.

Nonetheless, J. Gimeno et al. [14] experimentally measured and reported the macroscopic spray characteristics of this validation case (together with many other injection conditions). The spray tip penetration up to 60 mm is provided as well as the spray cone angle and the R-parameter. Since the focus of this study is the cavitation

R. Payri, J. Gimeno, P. Martí-Aldaraví, M. Martínez, "Validation of a three-phase Eulerian CFD model to account for cavitation and spray atomization phenomena", *Journal of the Brazilian Society of Mechanical Sciences and Engineering*, 43(228), pp. 1-15, 2021. DOI:0.1007/s40430-021-02948-z.

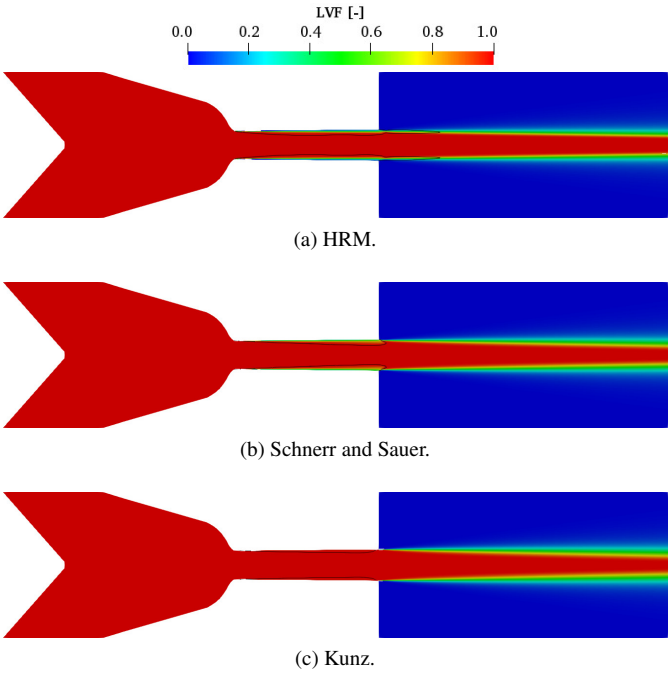

(a) HRM.

(b) Schnerr and Sauer.

(c) Kunz.

Fig. 11: Liquid volume fraction contours of the "Spray C" validation case.

phenomenon, the computational domain was not prepared to simulate the complete spray evolution, leaving the spray cone angle and the R-parameter as comparison metrics. Definitions of these two are [14]:

- Spray cone angle (θ). It is obtained from the liquid mass fraction contour of Figure 12. Since the spray occupies the complete computational domain from the first milliseconds of the simulation, the spray angle is estimated as the angle of the trapezium (white lines) whose bases are the segments inside the 0.01 liquid mass fraction contour that coincide with distances 12% and 50% (black lines) of the computational domain length, as skectched in also Figure 12.
- R-parameter. It is a parameter based on the spray injection theory under the assumption of conical shaped spray. During the steady-state injection, the spray penetration is proportional to the square root of time (see Equation 24), therefore, taking the spray angle and the momentum flux as constants from this stabilization point, the derivative of the spray penetration respect to the square root of time must be constant too, as shown in Equation 24.

$$S(t) \propto \dot{M}^{\frac{1}{4}} \rho_g^{-\frac{1}{4}} \tan^{-\frac{1}{2}}\left(\frac{\theta}{2}\right) t^{\frac{1}{2}} \rightarrow \text{R-parameter} = \frac{\partial S(t)}{\partial \sqrt{t}} \equiv \text{cte} \qquad (24)$$

Experimental and computational values of these two metrics are listed in Table 6. Once again, the HRM is the model that more accurately predicts the spray cone angle, with an error within the experimental uncertainty. Even though differences are small,

R. Payri, J. Gimeno, P. Martí-Aldaraví, M. Martínez, "Validation of a three-phase Eulerian CFD model to account for cavitation and spray atomization phenomena", *Journal of the Brazilian Society of Mechanical Sciences and Engineering*, 43(228), pp. 1-15, 2021. DOI:0.1007/s40430-021-02948-z.

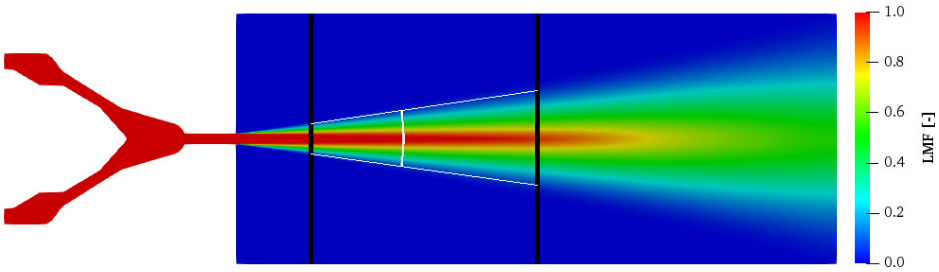

Fig. 12: Liquid mass fraction contours of the "Spray C" validation case performed with the HRM including reference lines for the spray cone angle definition.

the cavitation model that predicts higher discharge and momentum coefficients also provides wider spray angle. This is surprising because, as reported by researchers [33, 36], spray aperture angle substantially increases as cavitation is stronger. That is due to the collapse of vapor cavities, whose released energy increases momentum in the radial direction of the surrounding liquid. Then, the Schnerr and Sauer and Kunz models seem to overpredict the vapor bubble collapse outside the nozzle, even if they predict lower amount of fuel vapor inside of it, as shown in Figure 11.

Table 6: Steady-state spray cone angle and R-parameter of the "Spray C" validation case.

	θ [°]	R-parameter [m/s$^{0.5}$]
Experimental	17.78 ± 1.01	2.12 ± 0.18
HRM	18.76	2.82 ± 0.67
Schnerr and Sauer	20.42	2.70 ± 0.71
Kunz	20.42	2.72 ± 0.93

The experimental value of R-parameter has been obtained as the average between 0.2 ms and 0.8 ms after start of injection. On the other hand, the parameter for the simulations had to be averaged between 0.055 ms and 0.1 ms due to the limitation of the computational domain. The assumption of constant momentum flux and spray angle is not exactly fulfilled during this early time of the injection process. This explains the higher simulation average values, but also the higher standard deviation. In any case, experimental and all computational values are close taking into account the variability of the R-parameter. Comparing the three cavitation models, the HRM predicts faster spray penetration (slightly larger R-parameter), which is consistent with its smaller spray cone angle.

5 Conclusions

In this work, a three-phase CFD solver is developed and validated. The ESA model is updated in order to include the cavitation phase change phenomenon. The mod-

R. Payri, J. Gimeno, P. Martí-Aldaraví, M. Martínez, "Validation of a three-phase Eulerian CFD model to account for cavitation and spray atomization phenomena", *Journal of the Brazilian Society of Mechanical Sciences and Engineering*, 43(228), pp. 1-15, 2021. DOI:0.1007/s40430-021-02948-z.

ification is validated against experimental results in three distinct typical cavitation validation cases: a 2D throttle, a NACA 0015 hydrofoil, and a single-hole ECN reference diesel injector. The main characteristics of the presented model are:

- The homogeneous fluid approach is used for the three-phase mixture.
- It includes an atomization model valid for high *Re* and *We* numbers.
- It includes a cavitation phase-change model (which can be switched if necessary).
- Realistic thermodynamic properties for all fluids and phases are employed.

Three different cavitation sub-models are tested: HRM, Schnerr and Sauer, and Kunz. All of them include model constants which require optimization for each particular case. Instead, in this work, the optimized values from the literature are employed, modified from one validation case to another when needed (their value might be related with some fluid properties, but further research is needed to draw final conclusions on this):

- For the HRM, the exponents of the relaxation time expression are the same for all cases, the ones reported in the literature ($X_v^{-0.54}$ and $\psi^{-1.76}$). However, the relaxation time proportionality constant, θ_0, required to reproduce experimental results varies. It differs two orders of magnitude from wall bounded flows with n-dodecane ($\theta_0 = 3.84 \cdot 10^{-8}$ s, which is the default value according to the literature) to free flows with water ($\theta_0 = 3.84 \cdot 10^{-6}$ s), being smaller for cavitation of n-dodecane occurring within walls.
- For the Schnerr and Sauer model, the concentration of the cavitation nuclei has to be decreased several orders of magnitude from wall bounded flow with n-dodecane cases ($n_0 = 10^{13}$ m^{-3}, which is the value reported in the consulted literature) to free flow cases ($n_0 = 5 \cdot 10^8$ m^{-3}).
- The Kunz model itself includes two constants that depend on the simulated case, the characteristic velocity and the mean flow time scale. Using the proper values of these two ($C_{prod} = 3323$ and $C_{dest} = 4328$) allows the other constants to be the same for all cases.

Among the three tested models, the HRM reproduces the experimental results, in general, better than the Schnerr and Sauer and the Kunz models. For the 2D throttle validation case, the performance of the three of them is relatively similar. All of them overpredict the critical cavitation number (save that the fluid employed in the simulations is not exactly the same than the one used in the experiments), slightly overpredict the chocked mass flow, and clearly underpredict the area occupied by the vapor phase. For the NACA 0015 hydrofoil, the HRM is the only one that matches the experimental trend, even though it underpredicts the region of the suction side where steam is found. The same type of underprediction of the vapor phase region is observed in the single-hole ECN diesel injector. Its area coefficient, and therefore the discharge coefficient, are overpredicted, being the HRM the model that provides results closest to experimental data with an error of 7.8%. The liquid spray atomization and development can also be analyzed in this case, resulting that the predicted spray cone angle by this ESA model with the HRM matches the experimental result (it is within the experimental uncertainty).

R. Payri, J. Gimeno, P. Martí-Aldaraví, M. Martínez, "Validation of a three-phase Eulerian CFD model to account for cavitation and spray atomization phenomena", *Journal of the Brazilian Society of Mechanical Sciences and Engineering*, 43(228), pp. 1-15, 2021. DOI:0.1007/s40430-021-02948-z.

Therefore, the HRM is the proposed cavitation sub-model to be coupled to the ESA, since this combination is capable of reproducing the experimental findings with relatively good accuracy. The differences found between simulations and experiments are associated to the unsteady and turbulent nature of the cavitation phenomenon, fact also suggested by other researchers. Therefore, more accurate approaches for simulating the turbulence, such as Large Eddy Simulation (LES), could be used in the future to further improve the computational predictions.

References

1. Abbasiasl, T., Niazi, S., Aghdam, A.S., Chen, H., Cebeci, F.Ç., Ghorbani, M., Grishenkov, D., Koar, A.: Effect of intensified cavitation using poly(vinyl alcohol) microbubbles on spray atomization characteristics in microscale. AIP Advances **10**(2) (2020). DOI 10.1063/1.5142607
2. Arabnejad, M.H., Amini, A., Farhat, M., Bensow, R.E.: Numerical and experimental investigation of shedding mechanisms from leading-edge cavitation. International Journal of Multiphase Flow **119**, 123–143 (2019). DOI 10.1016/j.ijmultiphaseflow.2019.06.010
3. Bardi, M., Payri, R., Malbec, L.M., Bruneaux, G., Pickett, L.M., Manin, J., Bazyn, T., Genzale, C.L.: Engine Combustion Network: Comparison of Spray Development, Vaporization, and Combustion in Different Combustion Vessels. Atomization and Sprays **22**(10), 807–842 (2012). DOI 10.1615/AtomizSpr.2013005837
4. Battistoni, M., Duke, D.J., Swantek, A.B., Tilocco, F.Z., Powell, C.F., Som, S.: Effects of noncondensable gas on cavitating nozzles. Atomization and Sprays **25**(6), 453–483 (2015). DOI 10.1615/AtomizSpr.2015011076
5. Battistoni, M., Magnotti, G.M., Genzale, C.L., Arienti, M., Matusik, K.E., Duke, D.J., Giraldo, J., Ilavsky, J., Kastengren, A.L., Powell, C.F., Marti-Aldaravi, P.: Experimental and Computational Investigation of Subcritical Near-Nozzle Spray Structure and Primary Atomization in the Engine Combustion Network Spray D. SAE Technical Paper (2018-01-0277), 1–15 (2018). DOI 10.4271/2018-01-0277
6. Bilicki, Z., Kestin, J.: Physical Aspects of the Relaxation Model in Two-Phase Flow. Proceedings of the Royal Society A: Mathematical, Physical and Engineering Sciences **428**, 379–397 (1990). DOI 10.1098/rspa.1990.0040
7. Brusiani, F., Negro, S., Bianchi, G.M., Moulai, M., Neroorkar, K., Schmidt, D.P.: Comparison of the Homogeneous Relaxation Model and a Rayleigh Plesset Cavitation Model in Predicting the Cavitating Flow Through Various Injector Hole Shapes. SAE International (2013). DOI 10.4271/2013-01-1613
8. Cazzoli, G., Falfari, S., Bianchi, G.M., Forte, C., Catellani, C.: Assessment of the Cavitation Models Implemented in OpenFOAM® Under DI-like Conditions. Energy Procedia **101**, 638–645 (2016). DOI 10.1016/j.egypro.2016.11.081
9. Cervone, A., Bramanti, C., Rapposelli, E., D'Agostino, L.: Thermal cavitation experiments on a NACA 0015 hydrofoil. Journal of Fluids Engineering, Transactions of the ASME **128**, 326–331 (2006). DOI 10.1115/1.2169808
10. Coutier-Delgosha, O., Fortes-Patella, R., Reboud, J.L.: Evaluation of the turbulence model influence on the numerical simulations of unsteady cavitation. Journal of Fluids Engineering, Transactions of the ASME **125**, 38–45 (2003). DOI 10.1115/1.1524584
11. De Lorenzo, M., Lafon, P., Di Matteo, M., Pelanti, M., Seynhaeve, J.M., Bartosiewicz, Y.: Homogeneous two-phase flow models and accurate steam-water table look-up method for fast transient simulations. International Journal of Multiphase Flow **95**, 199–219 (2017). DOI 10.1016/j.ijmultiphaseflow.2017.06.001
12. Duke, D.J., Kastengren, A.L., Matusik, K.E., Powell, C.F.: Hard X-ray fluorescence spectroscopy of high pressure cavitating fluids in aluminum nozzles. International Journal of Multiphase Flow **108**, 69–79 (2018). DOI 10.1016/j.ijmultiphaseflow.2018.05.026
13. Gevari, M.T., Abbasiasl, T., Niazi, S., Ghorbani, M., Koar, A.: Direct and indirect thermal applications of hydrodynamic and acoustic cavitation: A review. Applied Thermal Engineering **171** (2020). DOI 10.1016/j.applthermaleng.2020.115065

14. Gimeno, J., Bracho, G., Martí-Aldaraví, P., Peraza, J.: Experimental study of the injection conditions influence over n-dodecane and diesel sprays with two ECN single-hole nozzles. Part I: Inert atmosphere. Energy Conversion and Management **126**, 1146–1156 (2016). DOI 10.1016/j.enconman.2016.07.077
15. Guo, G., He, Z., Zhang, Z., Duan, L., Guan, W., Duan, X., Jin, Y.: Visual experimental investigations of string cavitation and residual bubbles in the diesel nozzle and effects on initial spray structures. International Journal of Engine Research **21**(3), 437–447 (2020). DOI 10.1177/1468087418791061
16. bo Huang, H., Long, Y., Ji, B.: Experimental investigation of vortex generator influences on propeller cavitation and hull pressure fluctuations. Journal of Hydrodynamics **32**, 82–92 (2020). DOI 10.1007/s42241-020-0005-5
17. Issa, R.: Solution of the implicitly discretised fluid flow equations by operator-splitting. Journal of Computational Physics **62**(1), 40–65 (1986). DOI 10.1016/0021-9991(86)90099-9. URL http://www.eng.newcastle.edu.au/ jhb519/teaching/caut1/Apuntes/PID.pdf https://linkinghub.elsevier.com/retrieve/pii/0021999186900999
18. Jahangir, S., Wagner, E.C., Mudde, R.F., Poelma, C.: Void fraction measurements in partial cavitation regimes by X-ray computed tomography. International Journal of Multiphase Flow **120**, 103085 (2019). DOI 10.1016/j.ijmultiphaseflow.2019.103085
19. Kastengren, A.L., Tilocco, F.Z., Powell, C.F., Manin, J., Pickett, L.M., Payri, R., Bazyn, T.: Engine Combustion Network (ECN): Measurements of Nozzle Geometry and Hydraulic Behavior. Atomization and Sprays **22**(12), 1011–1052 (2012). DOI 10.1615/AtomizSpr.2013006309
20. Kirsch, V., Hermans, M., Schönberger, J., Ruoff, I., Willmann, M., Reisgen, U., Kneer, R., Reddemann, M.A.: Transparent high-pressure nozzles for visualization of nozzle internal and external flow phenomena. Review of Scientific Instruments **90**, 033702 (2019). DOI 10.1063/1.5065658
21. Koukouvinis, P., Gavaises, M., Li, J., Wang, L.: Large Eddy Simulation of Diesel injector including cavitation effects and correlation to erosion damage. Fuel **175**, 26–39 (2016). DOI 10.1016/j.fuel.2016.02.037
22. Kunz, R.F., Boger, D.A., Stinebring, D.R., Chyczewski, T.S., Gibeling, H.J., Venkateswaran, S., Govindan, T.R.: A preconditioned navier-stokes method for two-phase flows with application to Cavitation prediction. Computers & Fluids **29**, 849–875 (2000). DOI 10.2514/6.1999-3329
23. Kunz, R.F., Stinebring, D.R., Chyczewski, T.S., Boger, D.A., Gibeling, H.J., Govindan, T.R.: Multiphase CFD analysis of natural and ventilated cavitation about submerged bodies. In: FEDSM'99, 3rd ASME/JSME Joint Fluids Engineering Conference. San Francisco (1999)
24. Li, D., Kang, Y., Ding, X., Liu, W.: Experimental study on the effects of feeding pipe diameter on the cavitation erosion performance of self-resonating cavitating waterjet. Experimental Thermal and Fluid Science **82**, 314–325 (2017). DOI 10.1016/j.expthermflusci.2016.11.029
25. Li, M., Yao, J., Lan, B., Sankin, G., Zhou, Y., Liu, W., Xia, J., Wang, D., Trahey, G., Zhong, P.: Simultaneous Photoacoustic Imaging and Cavitation Mapping in Shockwave Lithotripsy. IEEE Transactions on Medical Imaging **39**(2), 468–477 (2020). DOI 10.1109/TMI.2019.2928740
26. Menter, F.R.: Improved two-equation k-omega turbulence models for aerodynamic flows. Tech. rep. (1992)
27. Morgut, M., Nobile, E., Biluš, I.: Comparison of mass transfer models for the numerical prediction of sheet cavitation around a hydrofoil. International Journal of Multiphase Flow **37**(6), 620–626 (2011). DOI 10.1016/j.ijmultiphaseflow.2011.03.005
28. NIST: NIST Chemistry WebBook (2018). DOI 10.18434/T4D303. URL https://webbook.nist.gov/chemistry/fluid/
29. Obeid, S., Jha, R., Ahmadi, G.: RANS simulations of aerodynamic performance of NACA 0015 flapped airfoil. Fluids **2**(1) (2017). DOI 10.3390/fluids2010002
30. Payri, R., Gimeno, J., Cuisano, J., Arco, J.: Hydraulic characterization of diesel engine single-hole injectors. Fuel **180**, 357–366 (2016). DOI 10.1016/j.fuel.2016.03.083
31. Payri, R., Gimeno, J., Martí-Aldaraví, P., Alarcón, M.: A new approach to compute temperature in a liquid-gas mixture. Application to study the effect of wall nozzle temperature on a Diesel injector. International Journal of Heat and Fluid Flow **68**, 79–86 (2017). DOI 10.1016/j.ijheatfluidflow.2016.12.008
32. Payri, R., Gimeno, J., Martí-Aldaraví, P., Carreres, M.: Assessment on Internal Nozzle Flow Initialization in Diesel Spray Simulations. SAE Technical Paper 2015-01-0921 (2015). DOI 10.4271/2015-01-0921
33. Payri, R., Salvador, F.J., Gimeno, J., De la Morena, J.: Study of cavitation phenomena based on a technique for visualizing bubbles in a liquid pressurized chamber. International Journal of Heat and Fluid Flow **30**(4), 768–777 (2009). DOI 10.1016/j.ijheatfluidflow.2009.03.011

R. Payri, J. Gimeno, P. Martí-Aldaraví, M. Martínez, "Validation of a three-phase Eulerian CFD model to account for cavitation and spray atomization phenomena", *Journal of the Brazilian Society of Mechanical Sciences and Engineering*, 43(228), pp. 1-15, 2021. DOI:0.1007/s40430-021-02948-z.

34. Payri, R., Salvador, F.J., Gimeno, J., Venegas, O.: Study of cavitation phenomenon using different fuels in a transparent nozzle by hydraulic characterization and visualization. Experimental Thermal and Fluid Science **44**, 235–244 (2013). DOI 10.1016/j.expthermflusci.2012.06.013
35. Rachakonda, S.K., Wang, Y., Grover, R.O., Moulai, M., Baldwin, E., Zhang, G., Parrish, S., Diwakar, R., Kuo, T.W., Schmidt, D.P.: A computational approach to predict external spray characteristics for flashing and cavitating nozzles. International Journal of Multiphase Flow **106**, 21–33 (2018). DOI 10.1016/j.ijmultiphaseflow.2018.04.012
36. Ro, S., Kim, B., Park, S., Kim, Y.B., Choi, Byungchul, Jung, S., Lee, D.W.: Internal caviating flow and external spray behavior characteristics according to length-to-width ratio of transparent nozzle orifice. International Journal of Automotive Technology **21**(1), 181–188 (2020). DOI 10.1007/s12239-020-0018-7
37. Saha, K., Som, S., Battistoni, M.: Parametric Study of HRM for Gasoline Sprays. ILASS Americas 28th Annual Conference on Liquid Atomization and Spray Systems, Dearborn, MI, May 2016 (May) (2016)
38. Salvador, F.J., Carreres, M., Jaramillo, D., Martínez-López, J.: Comparison of microsac and VCO diesel injector nozzles in terms of internal nozzle flow characteristics. Energy Conversion and Management **103**, 284–299 (2015). DOI 10.1016/j.enconman.2015.05.062
39. Salvador, F.J., Gimeno, J., Pastor, J.M., Martí-Aldaraví, P.: Effect of turbulence model and inlet boundary condition on the diesel spray behavior simulated by an eulerian spray atomization (ESA) model. International Journal of Multiphase Flow **65**, 108–116 (2014). DOI 10.1016/j.ijmultiphaseflow.2014.06.003
40. Schnerr, G., Sauer, J.: Physical and numerical modeling of unsteady cavitation dynamics. In: ICMF-2001, 4th Internationl Conference on Multiphase Flow. New Orleans (2001)
41. Shahangian, N., Sharifian, L., Uehara, K., Noguchi, Y., Martinez, M., Marti-aldaravi, P., Payri, R.: Transient nozzle flow simulations of gasoline direct fuel injectors. Applied Thermal Engineering p. 115356 (2020). DOI 10.1016/j.applthermaleng.2020.115356. URL https://doi.org/10.1016/j.applthermaleng.2020.115356
42. SNL: Engine Combustion Network (ECN) (2019). URL ecn.sandia.gov/
43. Torregrosa, A.J., Payri, R., Javier Salvador, F., Crialesi-Esposito, M.: Study of turbulence in atomizing liquid jets. International Journal of Multiphase Flow **129**, 103328 (2020). DOI 10.1016/j.ijmultiphaseflow.2020.103328
44. Vallet, A., Burluka, A.A., Borghi, R.: Development of a eulerian model for the "atomization" of a liquid jet. Atomization and Sprays **11**(6), 619–642 (2001). DOI 10.1002/fld.1650080906
45. Wallis, G.B.: One-dimensional two-phase flow. McGraw-Hill Education (1969)
46. Weller, H.G., Tabor, G., Jasak, H., Fureby, C.: A tensorial approach to computational continuum mechanics using object-oriented techniques. Computers in Physics **12**(6), 620–631 (1998). DOI 10.1063/1.168744
47. Wilcox, D.C.: Reassessment of the scale-determining equation for advanced turbulence models. AIAA Journal **26**(11), 1299–1310 (1988). DOI 10.2514/3.10041
48. Wilcox, D.C.: Formulation of the k-ω turbulence model revisited. AIAA Journal **46**(11), 2823–2838 (2008). DOI 10.2514/1.36541
49. Winklhofer, E., Kull, E., Kelz, E., Morozov, A.: Comprehensive hydraulic and flow field documentation in model throttle experiments under cavitation conditions. In: ILASS-Europe. Zurich (2001). DOI 10.13140/2.1.1716.4161
50. Yu, A., Luo, X., Yang, D., Zhou, J.: Experimental and numerical study of ventilation cavitation around a NACA0015 hydrofoil with special emphasis on bubble evolution and air-vapor interactions. Engineering Computations (Swansea, Wales) **35**(3), 1528–1542 (2018). DOI 10.1108/EC-01-2017-0020
51. Yu, A., Tang, Q., Zhou, D.: Cavitation evolution around a NACA0015 hydrofoil with different cavitation models based on level set method. Applied Sciences **9**, 758–771 (2019). DOI 10.3390/app9040758
52. Zhou, H., Xiang, M., Okolo, P.N., Wu, Z., Bennett, G.J., Zhang, W.: An efficient calibration approach for cavitation model constants based on OpenFOAM platform. Journal of Marine Science and Technology **24**, 1043–1056 (2019). DOI 10.1007/s00773-018-0604-9
53. Zhou, H., Xiang, M., Zhao, S., Zhang, W.: Development of a multiphase cavitation solver and its application for ventilated cavitating flows with natural cavitation. International Journal of Multiphase Flow **115**, 62–74 (2019). DOI 10.1016/j.ijmultiphaseflow.2019.03.020
54. Zwart, P.J., Gerber, A.G., Belamri, T.: A two-phase flow model for predicting cavitation dynamics. In: ICMF 2004 International Conference on Multiphase Flow. Yokohama (2004)

R. Payri, J. Gimeno, P. Martí-Aldaraví, M. Martínez, "Validation of a three-phase Eulerian CFD model to account for cavitation and spray atomization phenomena", *Journal of the Brazilian Society of Mechanical Sciences and Engineering*, 43(228), pp. 1-15, 2021. DOI:0.1007/s40430-021-02948-z.